GNSS-Based Passive Radar for Maritime Surveillance: Long Integration Time MTI Technique

F. Pieralice, F. Santi, D. Pastina
Department of Information Engineering, Electronics and Telecommunications
University of Rome "La Sapienza"
Rome, Italy
pieralice@diet.uniroma1.it
santi@diet.uniroma1.it
debora@infocom.uniroma1.it

M. Bucciarelli
Sympas s.r.l.
Viale Giulio Cesare, 71
Rome, Italy
bucciarelli@sympas-srl.it

H. Ma, M. Antoniou, M. Cherniakov
School of Electronic, Electrical and System Engineering
University of Birmingham"
Birmingham, U.K.
h.ma.1@bham.ac.uk
m.antoniou@bham.ac.uk
m.cherniakov@bham.ac.uk

***Abstract*—The exploitation of the Global Navigation Satellite Systems (GNSS) as transmitters of opportunity in passive radar systems for maritime surveillance is particularly attractive because of the main advantages consisting in a global coverage (even in open sea) and in the availability of multiple sources (different satellites and constellations). The main drawback stays in the restricted power budget provided by navigation satellites. This makes necessary to conceive, define and develop innovative moving target detection techniques specifically tailored for the system under consideration, in order to make this technology a powerful tool for persistent surveillance of sea areas of interest. To this aim, a long integration time Maritime Moving Target Indication technique is proposed in this work, and its effectiveness is proved against experimental data involving a small maritime target, not detectable by conventional MTI techniques. Obtained results prove the feasibility of a maritime MTI mode for GNSS based passive systems.**

Keywords—Maritime Moving Target Indication (M-MTI), passive radar, GNSS-based radar, maritime surveillance

I. INTRODUCTION

Keeping safe the sea environment is one of the biggest challenges of the last years. A large number of human activities takes place in maritime domain, varying from cruising and fishing up to nefarious activities such as piracy, human smuggling or terrorist actions. Radar sensors are intensively used in the framework of the maritime surveillance, due to their capability to acquire data autonomously and continuatively, night and day and under all weather conditions. Motivated by the well-known benefits of passive radars, an increasing number of studies have been dedicated to the exploitation of opportunistic sources for maritime surveillance applications. A variety of systems has been proposed based on terrestrial transmitters, such as DVB-T [1]-[3] and GSM [4], representing a cost-competing solution for the Sea Border surveillance. However, terrestrial sources cannot provide coverage of open sea areas. To such a purpose, satellite sources, such as DVB-S [5] and Inmarsat [6], have to be considered.

A very promising option is to exploit the signal transmitted by Global Navigation Satellite Systems (GNSS), such as GPS, GLONASS and the forthcoming Galileo and BeiDou.

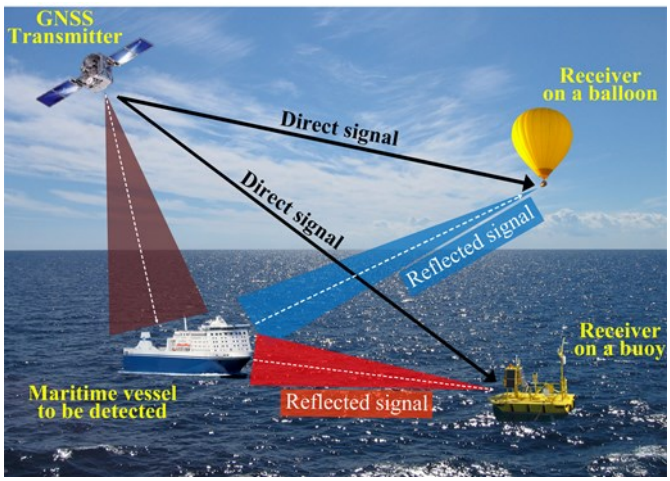

Fig. 1. System concept for GNSS-based radar for maritime surveillance.

Secondary use of these systems for remote sensing applications has been intensively investigated in the field of reflectometry (GNSS-R) from more than twenty years [7]. Concerning radar sensors, GNSS have been successfully employed in passive bistatic and multistatic Synthetic Aperture Radar, providing a powerful tool for persistent Earth observation and monitoring [8]-[11]. Furthermore, they have been considered for the detection of aerial targets [12] using a forward scattering geometry.

The focus here is on a GNSS-based passive radar for maritime surveillance in general bistatic geometries. The concept is illustrated in Fig. 1, where possible configurations involving a receiver mounted on a sea buoy and on a balloon above the sea have been sketched. From the radar perspective, there are a number of benefits deriving from the choice of these sources [8]. In particular, as well as the global coverage, a single GNSS constellation guarantees that every point over the Earth surface is constantly illuminated by 6-8 satellites, enabling multistatic acquisition able to increase the system performance [10], [11].

The main issue of this technology is the very restricted power budget. Indeed, EIRP levels of GNSS are very low, providing a power flux density near the Earth surface in the order of 3×10^{-14} W/m^2 [13]. This makes conventional techniques used in other types of passive radar based on terrestrial transmitters not directly applicable to the system under consideration, unless high Radar Cross Section (RCS) targets are considered. The feasibility of this novel application of GNSS for passive radar is demonstrated in a companion paper [14] by experimental data considering large vessels, i.e. high RCS targets. However, a key point of the GNSS-based passive radar is the definition of proper strategies to reach an acceptable level of signal to disturbance power ratio in order to allow target detection, independently on its dimension or distance from the receiver.

In this frame, this paper proposes a new long integration time processing technique enabling the Maritime-Moving Target Indication (M-MTI) capability for the GNSS-based passive radar. Such a technique defines a proper integration strategy of the received signal over long time intervals (in the order of 1 min), thus counteracting the restricted power budget provided by the GNSS. The effectiveness of the proposed technique is initially verified against synthetic data and then it is confirmed against experimental data considering a GLONASS transmitter and a small cooperative fishing ship.

The paper is organized as follows: an overview of the system is given in Section II and the proposed M-MTI technique is described in Section III. Synthetic and experimental results are shown in Section IV and Section V, respectively. Section VI concludes the paper.

II. SYSTEM OVERVIEW

The operative conditions are given by a GNSS transmitter and a parasitic receiver (see Fig. 1). The receiver is equipped with two RF channels. The former (Radar Channel RC) collects the signal reflections from the marine area to be surveyed, whereas the latter (Heterodyne Channel HC) records the direct signal transmitted by the satellite.

After quadrature demodulation and radar data reformatting according to an equivalent Pulse Repetition Interval (PRI), the RC signal can be compressed by a correlation with a noise-free replica of the reference signal, which can be regenerated according to direct signal parameters tracked by the HC,[14]. The range-compressed data in the fast-time&slow-time (t, u) domain can be written as

$$rc(t,u) = R_{cf}[t - \Delta\tau(u)] \times \exp\{j[2\pi\Delta f_d(u)t + \Delta\varphi(u)]\} \quad (1)$$

where $t \in [0, PRI]$ and $u \in \left[-{}^{T}/_{2}, {}^{T}/_{2}\right]$, being PRI typically set but not limited to be the duration of the ranging code and T the entire dwell time on target (usually several tens or hundreds of seconds long). $R_{cf}(\cdot)$ is the cross correlation function between the HC and RC signal. $\Delta\tau(u)$, $\Delta f_d(u)$ and $\Delta\varphi(u)$ are the instantaneous difference between direct and reflected signals in terms of delay, Doppler and phase. By selecting a proper Coherent Processing Interval (CPI) applying a Fast Fourier Transform (FFT) along the slow-time dimension, a Range Doppler (RD) map can be obtained, where the target could be distinguished from the stationary background as well as from the sea clutter returns thanks to the coherent processing gain.

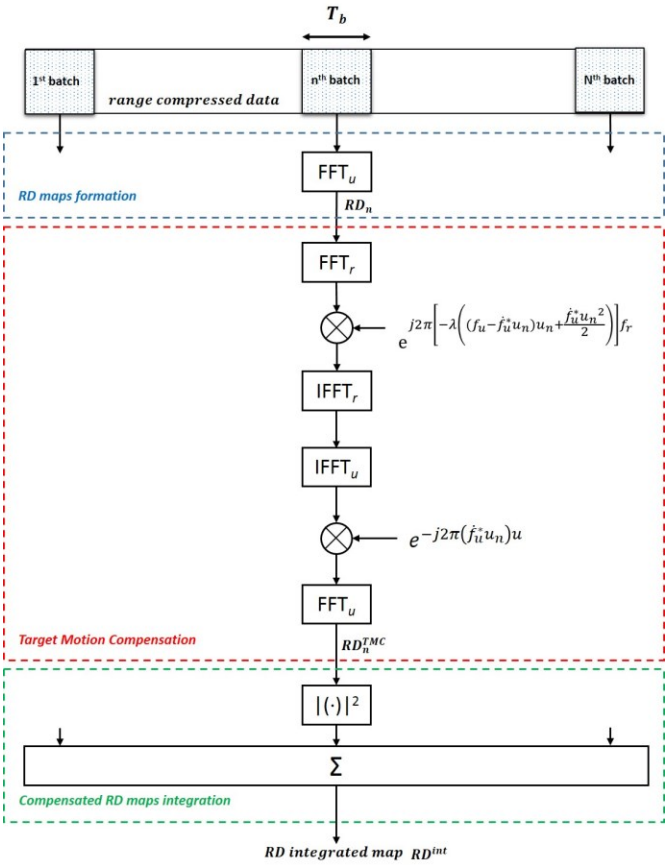

Fig. 2 Long integration time M-MTI processing scheme.

As experimentally proved in [14], targets with large RCS at relatively short receiver-target ranges can be successfully detected by considering CPIs in the order of 2-3s. Nevertheless, targets with medium/low RCS and/or at higher ranges need longer integration times to collect enough signal power to compete with the disturbance contributions. In such a condition, increasing the CPI over which the RD map is obtained would provoke high losses, making impossible the target detection, essentially for two reasons. First, the scattering mechanism could no more be regarded as coherent. Moreover, target motion over too long dwell times would give rise to both range and Doppler migrations, entailing a spread of the target energy over multiple RD cells. For these reasons, an innovative M-MTI technique able to deal with long integration times is here proposed, as described in the following section.

III. LONG INTEGRATION TIME MTI TECHNIQUE

The block diagram of the proposed technique is shown in Fig. 2. The technique receives as input the range-compressed RC data, and provides in output a RD map obtained over the entire dwell time T where the target can be likely detected thanks to the recovery of a suitable signal energy. The overall processing chain comprises three steps:

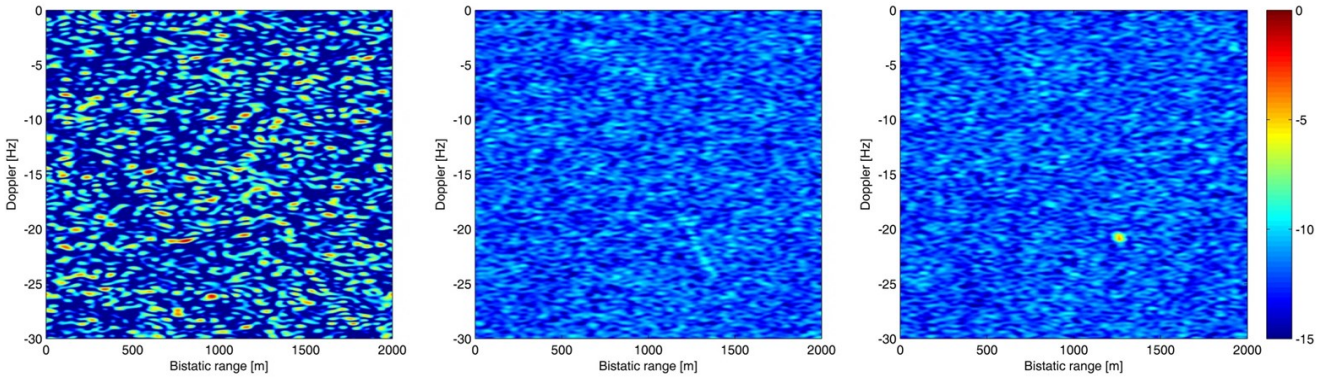

(a) (b) (c)

Fig. 3. Simulated results: (a) RD map of 3 s coherent integration time; (b) non-coherent summation of 20 RD maps without TMC; (c) non-coherent summation of 20 RD maps with TMC, with a total data acquisition time of 60 s.

1. RD maps formation – The entire dwell time is segmented in N consecutive batches of duration T_b, i.e.,

$$rc_n(t,u) = rc(t,u) \times rect_{T_b}(u - u_n) \qquad (2)$$

where $n = -\frac{N}{2}, \dots, \frac{N}{2} - 1$ and $u_n = nT_b + \frac{T_b}{2}$ is the slow-time instant over which the nth batch is centered. Imposing a limited batch duration, both constant target reflectivity and negligible range and Doppler migration can be assumed. According to the results in [14], these can be fulfilled by setting T_b equal to 2-3 s. Therefore, a FFT along the slow-time dimension can be applied to the individual batches (hence, $T_b = CPI$), thus obtaining a sequence of N RD maps.

2. Target Motion Compensation (TMC) – Due to target motion, the target will be differently located in the different RD maps. Therefore, range and Doppler migrations have to be compensated in order to perform an integration of the target returns over the entire dwell time.

Let (r^0, f_u^0) the range and Doppler reference position of the target evaluated at the reference time chosen to be $u = 0$s and let RD_n be the map pertaining the nth batch, where the target is located in $\left(r^{u_n}, f_u^{u_n}\right)$. With respect to the reference position, a range migration given by

$$\Delta r^n\left(f_u^n, \dot{f}_u^*\right) = r^{u_n} - r^0 =$$

$$= -\lambda\left[\left(f_u^{u_n} - \dot{f}_u^* u_n\right)u_n + \dot{f}_u^* \frac{{u_n}^2}{2}\right] \qquad (3)$$

is experienced, whereas the Doppler migration is equal to

$$\Delta f_u^n\left(\dot{f}_u^*\right) = f_u^{u_n} - f_u^0 = \dot{f}_u^* u_n. \qquad (4)$$

$\dot{f}_u^*$ is the target Doppler rate, assumed constant during the dwell time, and λ is the transmitted wavelength. Therefore, range migration can be compensated by multiplying the nth map in the (range frequency f_r, Doppler frequency f_u) domain for a phase term according to (3), whereas the Doppler migration is corrected in the (range r, slow-time u) domain by the phase term according to (4), as depicted in Fig. 2. At the end of the TMC procedure, a set of range&frequency aligned maps is obtained.

3. RD maps integration – Let $RD_n^{TMC}\left(r, f_u; \dot{f}_u^*\right)$ be the RD map pertaining the nth batch after the TMC procedure. The N resulting maps can be non-coherently integrated thus obtaining the final integrated map, i.e.

$$RD^{int}\left(r, f_u; \dot{f}_u^*\right) = \frac{1}{N}\sum_n \left|RD_n^{TMC}\left(r, f_u; \dot{f}_u^*\right)\right|^2. \qquad (5)$$

Thanks to the integration processing gain, the moving target can likely compete with the disturbance contributions and therefore it can be detected, for example by applying a 2D CA-CFAR (Cell Averaging Constant False Alarm Rate) detector.

It should be pointed out that the procedure described above depends on the specific target Doppler rate $\dot{f}_u$. Therefore, a completely adaptive technique has to take into account a bank performing TMC according to a specific set of Doppler rate values.

IV. SIMULATED RESULTS

A simulated analysis has been conducted to verify the effectiveness of the proposed technique. Parameters assumed in the simulations are in agreement with the parameters concerning the experimental trials described in the following. A GLONASS transmitter illuminates an area covered by the footprint of the radar antenna of a ground-based receiver and a point-like target moves in its field of view. At the reference instant $u = 0$s, the target is along the radar Line-of-Sight (LOS) at a distance of 1300 m moving with a velocity of 15 kt with heading angle 135° (measured counter-clockwise from the LOS direction). As disturbance, an additive white Gaussian noise is assumed occupying the useful signal bandwidth, with noise figure 1.5 dB and noise temperature 290 K. In addition, we assume the receiver equipped with a radar antenna having effective area equal to 0.14 m^2. Taking into account 6 dB of system losses, for a target with RCS = 24 dB a SNR of about -25 dB after range compression ($PRI = 1$ ms, [8]) is achieved.

One minute of dwell time is considered and, by setting $T_b = 3$ s, $N = 20$ batches are obtained. Fig. 3 shows the results of the MTI processing, where 0 dB represents the maximum intensity values among the three maps. Fig. 3(a) shows the RD map concerning the central batch, where it is evident how the target

is still buried in the disturbance background. Fig. 3(b) shows the integrated RD map obtained by skipping the TMC procedure. Even though a lower variance of the noise has been obtained because of the non-coherent integration, the target energy has not been correctly concentrated due to the range and Doppler migration over the integration time and consequently the target cannot be detected. Finally, Fig. 3(c) shows the integrated map accounting for the TMC step. As it is apparent, target energy has been well concentrated in a single RD location. Consequently, the proposed method can greatly enhance the ship detection capability of the GNSS-based passive radar. An example is in order to quantify the shown benefit. Considering the same disturbance power and RCS as in the previous simulation, fixing the probability of false alarm $P_{fa}=10^{-3}$, a numerically evaluated probability of detection not lower than $P_d=0.9$ can be achieved for target to receiver ranges up to ~1100 m, if the detection is performed over a single batch. To achieve the same performance in terms of P_d and P_{fa}, the proposed technique allows extending the maximum range up ~3100 m if the dwell time is set equal to 60 s (also taking onto account a set of 100 RD^{int} maps resulting for different possible values of the target Doppler rate).

(a)

(b)

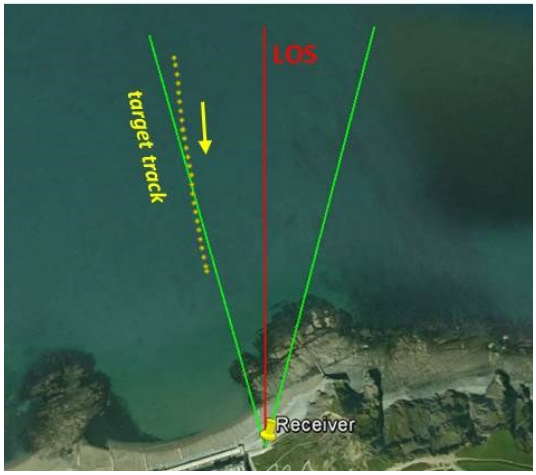

(c)

Fig. 4 Maritime experimental campaign – a) target of opportunity, b) receiving hardware, c) acquisition geometry.

TABLE I. EXPERIMENTAL AND SIGNAL PROCESSING PARAMETERS

Parameter		Unit	Value
Satellite	number	-	732
	carrier frequency	MHz	1603.6875
	azimuth (clockwise from N)	deg	3.0 ~ 6.8
	elevation	deg	73.2 ~ 73.1
Processing parameters	sampling frequency	MHz	50
	pulse repetition interval	ms	1
	dwell time	s	118
	batch duration (CPI)	s	3
	non-coherent processing interval	s	60

V. EXPERIMENTAL RESULTS

A maritime experimental campaign was conducted using GLONASS satellite as illuminator of opportunity with the passive receiver placed at the coastal area of Aberystwyth in UK. A fishing boat of length about 10 m was employed as target of opportunity [Fig. 4(a)]. A photograph of the experimental hardware is shown in Fig. 4(b). The real track of the fishing boat was recorded by a GPS receiver, which has been used as ground truth to validate the experimental results, see Fig. 4(c). During

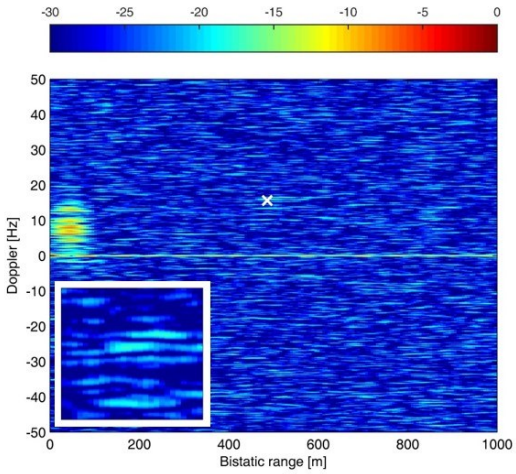

(a)

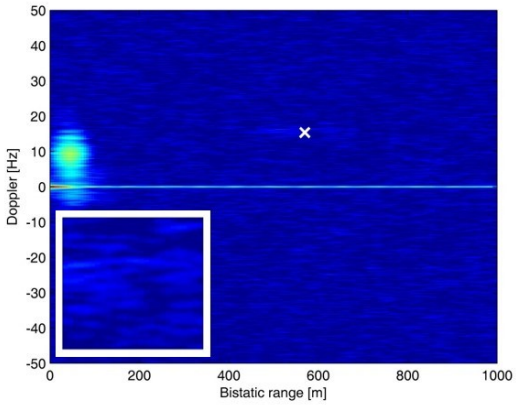

(b)

Fig. 5. Experimental results – a) single batch RD map, b) integrated RD map over 60 s without TMC.

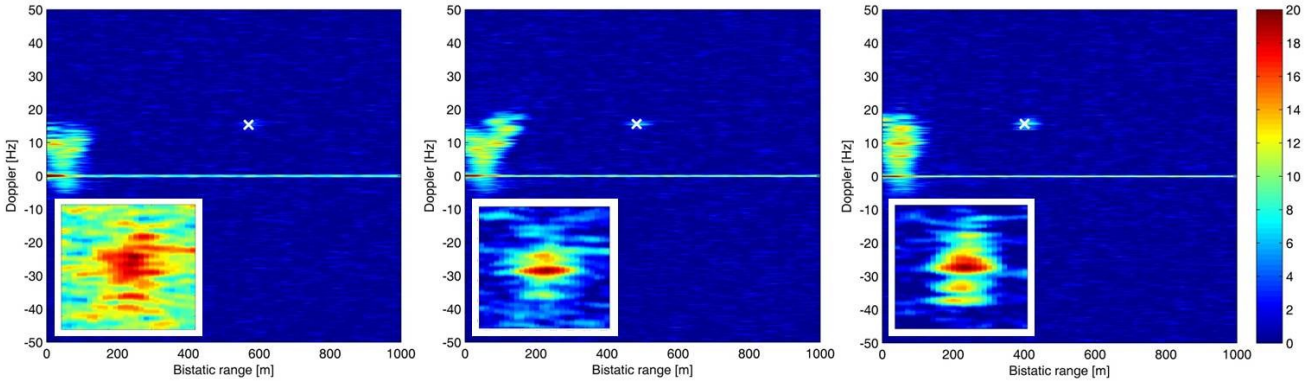

(a) (b) (c)

Fig. 6. Experimental RD integrated maps over T = 60 s – a) start time = 0 s, b) start time 30 s, c) start time 58 s.

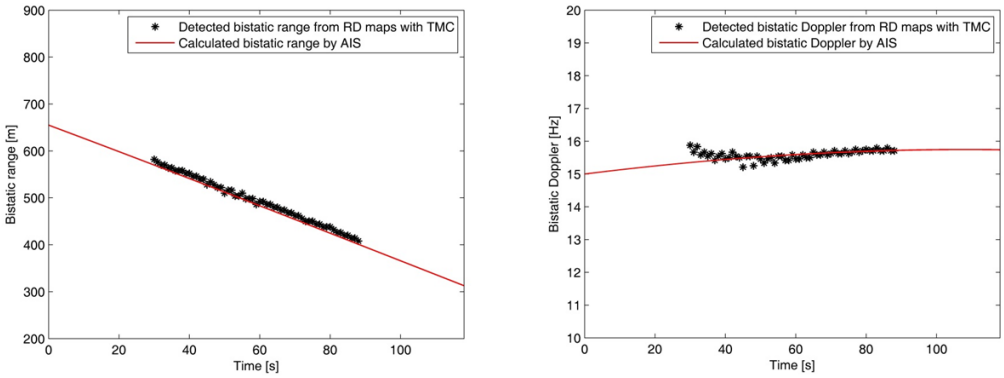

(a) (b)

Fig. 7. Detected range (a) and Doppler (b) history vs ground truth recorded by the GPS receiver.

the data collection, the ship was moving toward the receiver with a velocity of about 5 kt. Table I reports the acquisition and processing parameters.

Due to the small size of this target, the integration gain achieved over a single batch does not suffice to make the signal detectable. As example, Fig. 5(a) shows the RD map concerning the central batch of the acquisition. In the map, where 0 dB represents the highest echo intensity, the direct signal return at the zero-range zero-Doppler position as well as its sidelobes are well visible. Of course, such returns could be filtered out by proper cancellation processing [15], but in the presented analysis we chose to maintain them as comparison with the target echo as well as the sea clutter. A cluster of strong returns can be observed at approximately 50 m range, which could likely correspond to sea clutter echoes. The actual target position recorded by the GPS receiver is marked with a white "×" in the figure, and as it is apparent not any bright spot appears in such a region, as confirmed looking at the zoom showed in the bottom boxes. To improve the target signal energy, the non-coherent integration over the first 60 seconds of the acquisition has been performed, and the obtained integrated map is shown in Fig. 5(b). As it is apparent, the noise fluctuation has been greatly reduced by performing the integration, and a bright return appearing in the map could be reliably associated with a target by a CA-CFAR detector. However, this map has been obtained by skipping the TMC procedure. Therefore, target energy has not been correctly concentrated because of the range and Doppler migration, and neither in this case can the target be detected.

The previous analysis showed how a proper compensation of the target motion is mandatory to correctly build up the useful signal energy over long integration times. The TMC procedure described in Section III has been therefore taken into account, and the obtained results are shown in Fig. 6. To obtain the three RD integrated maps, a non-coherent processing interval of 60s, which corresponds to integrate 20 consecutive RD maps, has been selected with starting times 0s, 30s and 58s, respectively, and for the TMC the nominal Doppler rate value has been considered. In these figures, 0dB represents the background floor. A strong peak is clearly visible in all the maps in a RD position in good agreement with the actual target position as evaluated from the GPS measurements. Since the target is moving toward the receiver during the acquisition [see Fig. 4(c)], a higher signal to disturbance level is achieved for increasing start times. This can be well observed by looking at the three bottom boxes of Fig. 6, showing the patch of the maps containing the target return normalized to the peak position of each zoom. Thanks to the recovering of a proper signal to disturbance ratio, a CA-CFAR detector can at this point detect the target.

As it is apparent from Fig. 7, the peak position moves accordingly to the real target motion. This suggests the possibility to track the target position over the available dwell time. A time window of 60 s is considered moving along the observation time with a step of 1 s. Batches of duration 3 s are considered, and therefore 20 batches are integrated after the TMC procedure has been applied for each position of the time window. Thus, 59 integrated maps are obtained for the available 118 s of dwell time. For each one, the peak position corresponding to the target is recorded as detected bistatic range and Doppler position. Fig. 7 compared the detected range and Doppler history with the ground truth provided by the GPS receiver. As it is apparent, a very good coincidence between detected tracks and ground truth has been obtained. The Root Mean Square (RMS) of the difference between range and GPS reference is 8.73 m (with the range bin size equal to 6 m because of the sampling frequency of 50 MHz employed), whereas for the Doppler curves the RMS of the difference is 0.15 Hz (with the Doppler bin equal to $1/T_b \approx 0.3$ Hz). Obviously, a correct localization of the target on the ground plane could be obtained by exploiting multiple measurements made available from the exploitation of multiple satellites.

The above analysis confirmed that the proposed M-MTI technique is able to correctly collect the signal energy over long integration times (~1 min), thus allowing the GNSS-based passive radar not only to detect high-RCS vessels **Errore. L'origine riferimento non è stata trovata.**, but even low observable boats, thus increasing the detection performance of the proposed passive radar system.

VI. CONCLUSIONS

Our research aimed at the definition of a novel technology for maritime surveillance applications based on the exploitation of navigation satellites signals. The global coverage guaranteed by GNSS provides the potential of a persistent surveillance of every point over the Earth' surface, even in open sea scenarios, thus making this technology extremely appealing in the framework of Integrated Maritime Surveillance. Whilst in the companion paper [14] the system concept and a preliminary experimental validation have been presented against strong SNR data, here the focus has been on the definition of an advanced M-MTI mode able to counteract the low power density of the transmitted signal reaching the ground level, which represents the fundamental bottleneck of this technology for the detection of small and medium-long range targets.

Particularly, a Range&Doppler-based technique has been proposed able to concentrate the signal energy over integration times long enough to reach signal to disturbance levels suitable for the detection of maritime targets of small size. Results obtained against data collected during a maritime experimental campaign involving a GLONASS satellite and a small fishing boat showed the effectiveness of the proposed M-MTI technique to increase the detection capability of low observable targets. Because of the unfavorable power budget provided by the system under consideration, such a technique represents a key characteristic of the proposed technology.

Finally, it is worth to remark that one of the bigger benefits arising from the use of GNSS is the multitude of transmitters simultaneously illuminating the same area. Even though the case of a single transmitter has been here considered, it makes sense that the exploitation of multiple sources can greatly increase the performance of the proposed system, and this will be the focus of future steps of our research.

ACKNOWLEDGMENT

This project has received funding from the European GNSS Agency under the European Union's Horizon 2020 research and innovation program under grant agreement No 641486, "GALILEO-BASED PASSIVE RADAR SYSTEM FOR MARITIME SURVEILLANCE — spyGLASS". The first spyGLASS prototype will be an experimental van-mounted system designed and developed by Aster S.p.A. and Elettronica Gmbh.

REFERENCES

[1] D. W. O'Hagan, *et al*, "Passive bistatic radar (PBR) for harbour protection applications," *2012 IEEE Radar Conference*, Atlanta, GA, 2012, pp. 446-450.

[2] D. Langellotti, F. Colone, P. Lombardo, M. Sedehi, E. Tilli, "DVB-T based Passive Bistatic Radar for maritime surveillance," *2014 IEEE Radar Conference*, Cincinnati, OH, USA, 19–23 May 2014.

[3] T. Martelli, F. Colone, E. Tilli, A. Di Lallo, "Multi-frequency target detection techniques for DVB-T based passive radars sensors," *Sensors 2016*, 16 (10).

[4] R. Zemmari, M. Daun, M. Feldmann and U. Nickel, "Maritime surveillance with GSM passive radar: Detection and tracking of small agile targets," *14th Int. Radar Symp.*, Dresden, 2013, pp. 245-251.

[5] P. Marques, A. Ferreira, F. Fortes, P. Sampaio, H. Rebelo and L. Reis, "A pedagogical passive RADAR using DVB-S signals," *3rd Int. Asia-Pacific Conf. on Synthetic Aperture Radar*, Seoul, 2011, pp. 1-4.

[6] M. Golabi, A. Sheikhi, M. Biguesh, "A new approach for sea target detection in satellite based passive radar," *Iranian Conference on Electrical Engeneering*, Mashad, Iran, 2013, pp. 1-5

[7] M. Martìn-Neira, "A passive reflectometry and interferometry system (PARIS): Application to ocean altimetry," *ESA Journal* 17 (1993): 331-355.

[8] M. Antoniou and M. Cherniakov, "GNSS-based bistatic SAR: a signal processing view," *EURASIP J. Adv, Sign. Process*., 2013:98.

[9] H. Ma, M. Antoniou, M. Cherniakov, "Passive GNSS-based SAR resolution improvement using joint Galileo E5 signals," *IEEE Geosci. Remote Sens. Lett*., vol. 12, no. 8, pp. 1640-1644, Aug. 2015.

[10] F. Santi, M. Antoniou, D. Pastina, "Point spread function analysis for GNSS-based multistatic SAR," *IEEE Geosci. Remote Sens. Lett*., vol. 12, no. 2, pp. 304-308, Feb. 2015.

[11] F. Santi, M. Bucciarelli, D. Pastina, M. Antoniou, M. Cherniakov, "Spatial resolution improvement in GNSS-based SAR using multistatic acquisition and feature extraction," *IEEE Trans. Geosci. Remote Sens.*, vol. 54, no. 10, pp. 6217-6231, Oct. 2016.

[12] I. Suberviola, "Experimental results of air target detection using GPS forward-scattering radar," *IEEE Geosci. Remote Sens. Lett*, vol. 9, no. 1, pp. 47-51, Jan. 2012.

[13] X. He, M. Cherniakov, T. Zeng, "Signal detectability in SS-BSAR with GNSS non-cooperative transmitter," *IEE Proc. Radar Sonar Navig*., vol. 152, no. 3, pp.124-132, Jun. 2005.

[14] H. Ma, M. Antoniou, M. Chernaikov, *et al*., "Maritime target detection using GNSS-based radar: Experimental proof of concept," *Proc. of 2017 IEEE RadarConf*, Seattle, WA, USA, May 2017.

[15] F. Colone, D. W. O'Hagan, P. Lombardo and C. J. Baker, "A Multistage Processing Algorithm for Disturbance Removal and Target Detection in Passive Bistatic Radar," *IEEE Trans. Aerosp. Electr. Syst.*, vol. 45, no. 2, pp. 698-722, April 2009.